Draft version February 2, 2022
Typeset using LaTeX default style in AASTeX62

arXiv:1910.07996v1 [astro-ph.SR] 17 Oct 2019

Measurements of Low Temperature Rate Coefficients for the Reaction of CH with CH_2O and Application to Dark Cloud and AGB Stellar Wind Models.

Niclas A. West,[1] Tom J. Millar,[2,3] Marie Van de Sande,[4] Edward Rutter,[1] Mark A. Blitz,[1] Leen Decin,[4] and Dwayne E. Heard[1]

[1] *School of Chemistry, University of Leeds, Leeds, LS2 9JT, UK*
[2] *Astrophysics Research Centre, School of Mathematics and Physics, Queens University Belfast, University Road, Belfast BT7 1NN, UK*
[3] *Institute of Theory and Computation, Harvard-Smithsonian Center for Astrophysics, 60 Garden Street, Cambridge MA 02138, USA*
[4] *Instituut voor Sterrenkunde, KU Leuven, Celestijnenlaan 200D, 3001 Leuven, Belgium*

(Received July 23rd, 2019; Revised September 4th, 2019; Accepted September 26th, 2019)

Submitted to ApJ

ABSTRACT

Rate coefficients have been measured for the reaction of CH radicals with formaldehyde, CH_2O, over the temperature range 31 - 133 K using a pulsed Laval nozzle apparatus combined with pulsed laser photolysis and laser induced fluorescence spectroscopy. The rate coefficients are very large and display a distinct decrease with decreasing temperature below 70 K, although classical collision rate theory fails to reproduce this temperature dependence. The measured rate coefficients have been parameterized and used as input for astrochemical models for both dark cloud and AGB stellar outflow scenarios. The models predict a distinct change (up to a factor of two) in the abundance of ketene, H_2CCO, which is the major expected molecular product of the CH + CH_2O reaction.

Keywords: Astrochemistry (75) — Circumstellar envelopes (237) — Dense interstellar clouds (371) — Experimental techniques (2078) — Laboratory astrophysics (2004) — Reaction rates (2081)

1. INTRODUCTION

In order to adequately describe gas-phase astrochemistry within a model, it is necessary to have accurate knowledge of the rate coefficients for relevant species. Although progress has been made in the measurement of rate coefficients for neutral-neutral reactions at very low temperatures in the last 30 years since the invention of the CRESU technique (French acronym for Cinétique de Réaction en Ecoulement Supersonique Uniforme), there is still a limited database compared with those close to or above ∼298 K (Potapov et al. 2017). Theoretical prediction of rate coefficients at low temperatures is difficult owing to new reaction mechanisms sometimes becoming dominant at temperatures below ∼298 K. In addition, extrapolation of fits to experimental data above ∼298 K (Potapov et al. 2017; Heard 2018) can lead to errors in predicted rate coefficients at low temperatures. For some systems, rate coefficients continue to increase with a decrease in temperature down to the lowest temperatures accessible when using the CRESU technique (Cooke & Sims 2019). Indeed, the decrease in velocity with temperature often causes the importance of long-range molecular interactions to increase with a decrease in temperature. These mechanisms determine the temperature dependence of the reaction rate coefficient until it reaches the rate, called the collision limit, at which every collision of the reagent gas molecules leads to reaction. For some reactions, the collision limit is reached at temperatures relevant to the modeling of astrochemical environments (Smith et al. 2006b).

One reaction with a rate coefficient near the collision limit and showing an inverse temperature dependence at $T >$ 298 K is that of methylidyne (CH, also called carbyne) with formaldehyde (CH_2O). Methylidyne was one of the first molecules detected in the interstellar medium. Its optical absorption lines (see McKellar (1941) for a discussion of its

Corresponding author: Dwayne Heard
D.E.Heard@leeds.ac.uk

early history) were utilized to probe diffuse interstellar clouds while its radio wavelength transitions (Rydbeck et al. 1973) confirmed its presence in dense molecular clouds. It is now known to be widespread with detections in interstellar shock waves and external galaxies (Danks et al. 1984; Sandell et al. 1988; Muller et al. 2014). Similarly, formaldehyde, CH_2O, the first discovered organic polyatomic molecule (Snyder et al. 1969), is also an ubiquitous interstellar molecule, seen in almost all types of interstellar molecular cloud as well as in the circumstellar envelopes (CSEs) of C-rich and O-rich Asymptotic Giant Branch (AGB) stars. In this paper, we study the fast reaction between CH and CH_2O, the major molecular product of which is ketene, H_2CCO (Nguyen et al. 2014), and which is also a common molecule in dense interstellar clouds (Turner 1977; Matthews & Sears 1986; Ruiterkamp et al. 2007). Its formation can occur in the gas-phase via the radiative association $CH_3^+ + CO \longrightarrow H_3CCO^+ + h\nu$ followed by dissociative recombination with electrons. The UMIST Rate12 database also includes the neutral-neutral reaction $O + C_2H_3 \longrightarrow H_2CCO + H$ with a large rate coefficient, 1.6×10^{-10} cm^3 s^{-1} (Tsang & Hampson 1986), although this value is uncertain and may be a factor of 3 too large (Baulch et al. 2005). The KIDA database (Wakelam et al. 2015) adopts an overall rate coefficient of 1.1×10^{-10} cm^3 s^{-1} with channels to $H_2CCO + H$ (55%), $CH_3 + CO$ (36%) and $C_2H_2 + OH$ (9%). In recent years, it has also been suggested that ketene formation is via surface chemistry on icy grains followed by desorption to the gas phase (Hudson & Loeffler 2013; Maity et al. 2014).

Furthermore, CH and CH_2O have been observed in the atmospheres of Earth and Titan (Grosjean et al. 1993; Viskari et al. 2000; Saxena et al. 2003; Krasnopolsky 2009; Nixon et al. 2010; Atreya 2010) as well as in combustion processes (Fenimore 1971; Carlier et al. 1986; Miller & Bowman 1989; Anderson et al. 1996; Goulay et al. 2009). Although the reagents CH and CH_2O as well as the major molecular products H_2CCO, CH_3, and CO have been observed in low temperature astrochemical environments, the rate coefficients for the reaction of $CH + CH_2O$ have not been previously measured below 298 K.

CH, in its ground electronic state, $X^2\Pi$, is highly reactive because it has both an unpaired electron and a lone pair of electrons. Additionally, the relatively large dipole moments of CH and CH_2O (given in Section 3, Table 2) lead to stronger long-range interactions relevant to reaction mechanisms at low temperatures, making this an ideal system to study with the CRESU technique. Previously, Zabarnick et al. (1988) measured an inverse temperature dependence of the rate coefficient, $k_1(T)$, for the reaction of $CH + CH_2O$ at 298 K < T < 670 K by monitoring the rate of loss of CH via Laser-Induced Fluorescence (LIF). Subsequently, Nguyen et al. (2014) modeled the reaction with Variational Transition State Theory (VTST) and Rice-Ramsperger-Kassel-Marcus (RRKM) Master Equation calculations and determined that it proceeds through a barrierless potential energy surface which causes the negative temperature dependence of the reaction rate coefficients above 300 K, similar to other barrierless reactions (Phillips 1992). The authors also concluded that the primary pathways of the reaction were:

$$CH + CH_2O \xrightarrow{k_{1a}(T)} H + H_2CCO \ (\sim 82\% \text{ at } 300 \text{ K}, \Delta H_r^{\ominus} = \text{-}301.5 \text{ kJ mol}^{-1}), \tag{1a}$$

$$CH + CH_2O \xrightarrow{k_{1b}(T)} CH_3 + CO \ (\sim 16\% \text{ at } 300 \text{ K}, \Delta H_r^{\ominus} = \text{-}442.8 \text{ kJ mol}^{-1}), \tag{1b}$$

$$CH + CH_2O \xrightarrow{k_{1c}(T)} {}^3CH_2 + HCO \ (\lesssim 2\% \text{ at } 300 \text{ K}, \Delta H_r^{\ominus} = \text{-}53.2 \text{ kJ mol}^{-1}), \tag{1c}$$

where yields and enthalpies were calculated by Nguyen et al. (2014) at low pressures. Nguyen et al. (2014) also calculated that, above 300 K, the yield of channel 1a decreased with increasing temperature.

Previous reactions of CH with alkenes and alkynes measured with the CRESU technique have exhibited rate coefficients with a negative temperature dependence above $T \sim 60$ K, a maximum observed at $T \sim 60$ K, and a positive $\sim T^{1/6}$ dependence for $T \lesssim 60$ K (Canosa et al. 1997; Smith et al. 2006b). This $\sim T^{1/6}$ dependence was attributed to the rate coefficient reaching the collision limit as determined by Classical Capture Theory (CCT). CCT improves upon the simple hard sphere collision model by using orientation-averaged, attractive, long-range potentials between molecules in order to approximate the extent to which the intermolecular potentials would deflect the molecules. Since second-order rate coefficients can be described as:

$$k(T) = \sigma(T)\langle v(T)\rangle \tag{2}$$

where $k(T)$ and $\sigma(T)$ are the temperature-dependent rate coefficient (cm^{3}s^{-1}) and the temperature-dependent cross section (cm^2), respectively, for a given process such as reaction, collision, quenching, etc, and $\langle v(T)\rangle$ is the temperature-dependent average relative velocity (cm s^{-1}), the hard sphere collision rate has a temperature dependence of $T^{1/2}$ due entirely to the temperature dependence of $\langle v(T)\rangle$ since the hard sphere $\sigma(T)$ is temperature independent. However,

CCT predicts a different temperature dependence of the collision limit due to the dependence of $\sigma(T)$ on the form of the long-range attractive intermolecular potential. These potentials cause a larger deflection of molecules toward each other at low temperatures when average velocities of the molecules are slower, yielding a larger effective collision cross section. Unfortunately, the positive temperature dependence behavior of the reaction rate coefficients for CH with alkenes and alkynes measured by Canosa et al. (1997) and Smith et al. (2006b) were not well defined due to the behavior only occurring at the lowest temperature accessible by the CRESU apparatuses in these experiments (∼23 K). Therefore, the data were only fitted with the standard modified Arrhenius equation by Canosa et al. (1997) and Smith et al. (2006b); which has been previously expressed in two different forms:

$$k\left(T\right) = A\left(\frac{T}{\tau}\right)^{n} exp\left(-\frac{E_a}{RT}\right) \tag{3a}$$

$$k\left(T\right) = \alpha\left(\frac{T}{300}\right)^{\beta} exp\left(-\frac{\gamma}{T}\right), \tag{3b}$$

where A is a pre-exponential factor (cm^3s^{-1}), τ is usually either defined as ∼300 K or 1 K, n is a constant, E_a is the activation energy, R is the ideal gas constant, and α, β, and γ are versions of the parameters often utilized in astrochemical modeling. Since τ = 300 K is employed in the UMIST RATE12 and KIDA astrochemical databases, and τ = 1 K is often employed in fits of low temperature rate coefficients, the two types of fits can be converted using:

$$A_{\tau=300} = 300^{n} A_{\tau=1} \tag{4}$$

Since it is possible to fit experimental temperature dependencies with modified Arrhenius equations which have very different forms to those predicted by collision rate models (for instance a $\approx T^{1/6}$ dependence predicted by capture theory), Canosa et al. (1997) stated that their modified Arrhenius fit should not be extrapolated below 23 K, the lowest temperature measured in their experiments.

Several theoretical approaches have been developed to determine the temperature dependence of the collision limit. One method, CCT, predicts the rate coefficients of collisions controlled by the orientation-averaged long-range potential between two molecular species. Since the r^{-6} intermolecular potentials due to dipole-dipole ($D-D$), dipole-induced-dipole ($D-iD$), and London dispersion ($Disp$) forces yield a good first-order approximation of the long-range potential between the many neutral species, the collision rate coefficient predicted by CCT, $k_{coll}(T)$, is:

$$\begin{aligned} k_{coll}(T) &= \sigma_{coll}(T)\langle v(T)\rangle \\ &= \left[\pi\left(\frac{2C_6}{k_B T}\right)^{1/3}\Gamma\left(\frac{2}{3}\right)\right]\left[\left(\frac{8k_B T}{\pi\mu}\right)^{1/2}\right], \end{aligned} \tag{5}$$

where k_B is the Boltzmann constant, $\Gamma(x)$ is the gamma function such that $\Gamma(2/3) = 1.353$, μ is the reduced mass of the collision, and C_6 is the sum of coefficients describing the magnitude of the attractive forces between collision partners (J cm^6) (Smith 1980; Stoecklin et al. 1991). C_6 can be described by:

$$C_6 = C_6^{D-D} + C_6^{D-iD} + C_6^{Disp}, \tag{6}$$

with C_6^{D-D} described by:

$$C_6^{D-D} = \frac{2}{3}\left(\frac{\mu_1^2\mu_2^2}{k_B T(4\pi\epsilon_0)^2}\right), \tag{7}$$

where μ_1 and μ_2 are the dipole moments of reagents 1 and 2 and ϵ_0 is the permittivity of free space (Hirschfelder et al. 1964). C_6^{D-iD} can be described by:

$$C_6^{D-iD} = \frac{\mu_1^2\alpha_2 + \mu_2^2\alpha_1}{4\pi\epsilon_0}, \tag{8}$$

where α_1 and α_2 are the polarizabilities of reagents 1 and 2, and C_6^{Disp} is given by:

$$C_6^{Disp} = \frac{3}{2}\alpha_1\alpha_2\left(\frac{I_1 I_2}{I_1 + I_2}\right), \tag{9}$$

where I_1 and I_2 are the ionization energies of reagents 1 and 2. A number of other techniques have been applied when more accurate descriptions of the intermolecular potential have been needed (Phillips 1992). One technique, rotationally Adiabatic Capture (AC) theory, was developed to calculate the long-range $D-D$, and dipole-quadrupole ($D-Q$) intermolecular potential mostly between diatomic molecules (Stoecklin et al. 1991; Clary et al. 1993; Clary 1994). In AC theory, long-range intermolecular potentials for individual molecular rotational states are calculated and utilized to determine rate coefficients for each rotational state. These single quantum state rate coefficients are then averaged over a Maxwell-Boltzmann distribution in order to determine the final temperature-dependent collision rate coefficient. Such collision rate coefficients are found to go to zero at 0 K, increase as $\sim T^{1/6}$ above 0 K when only approximately one state is populated until reaching a maximum value, and then decrease as $\sim T^{-1/6}$ at higher temperatures when a many states are populated. The maximum value was reached at $\sim$ 1 K for simple diatom-diatom collisions, but the maximum was found to shift to $\sim$20 K when electronic effects were considered for OH + HBr, a $^2\Pi-\ ^1\Sigma$ system (Clary et al. 1993). For the reaction CH + NH_3, AC was able to calculate rate coefficients to within a factor of $\sim$2 of measured values below 100 K (Stoecklin & Clary 1995). In a somewhat similar technique, Statistical Adiabatic Capture Model (SACM), adiabatic intermolecular potentials are calculated in order to determine capture rate coefficients (Quack & Troe 1974; Troe 1985). Additionally, the technique of long-range E,J-resolved microcanonical Variational Transition State Theory (μj-VTST) should yield approximately the same low temperature rate coefficients as the AC and SACM techniques since the centrifugal barrier becomes the dominant transition state in the determination of the rate coefficient when the reaction has reached the collision limit (Georgievskii & Klippenstein 2005). μj-VTST was found to agree with experimental measurements to within a factor of $\sim$2 for the reaction of CN + O_2 and to within a factor of $\sim$5 for the reaction of CH + NH_3 near 20 K (Georgievskii & Klippenstein 2005).

In this paper the temperature-dependent rate coefficients for the reaction between CH + CH_2O were measured between 31 - 133 K and fitted with Equation 5, the collision limit derived from classical capture theory. The effects of employing the optimized fit was then determined in model predictions of the abundances of key species in AGB stellar winds and dark interstellar clouds.

2. EXPERIMENTAL METHOD

Low temperature kinetics measurements of the reaction CH + CH_2O were performed in a pulsed Laval nozzle apparatus, with the Pulsed Laser Photolysis - Laser Induced Fluorescence (PLP-LIF) technique, schematically shown in Figure 1. The reagent and CH precursor gases, formaldehyde and bromoform ($CHBr_3$) respectively, were prepared separately before being controllably mixed and directed to the Laval nozzle apparatus. Mixtures of formaldehyde and bath gases were prepared in cylinders, utilizing a similar method to those utilized in previous literature (Sivakumaran et al. 2003; Oliveira et al. 2016). Formaldehyde gas was generated by gently heating the polymerized form of formaldehyde, paraformaldehyde powder (Sigma-Aldrich, 95%), with a heat gun (Steinel, model HL1810S) to $\sim$70°C in an evacuated 500 mL glass bottle (Duran) modified to be leak-tight and connected to a vacuum line. The formaldehyde gas was passed through a cold trap which was submerged in ethanol (VWR, 99.96%) chilled to -10°C with a refrigerated immersion probe (LaPlant, model 100CD) in order to trap any water or other condensable byproducts. Empty cylinders attached to the vacuum line were then filled with the purified formaldehyde gas to $\sim$200 Torr ($\sim$26.7 kPa) and then argon (BOC, 99.998%) or nitrogen (BOC, 99.998%) gas was added to $\sim$6 atm ($\sim$608 kPa) creating $\sim$4.4% mixtures of formaldehyde gas. The cylinders were then left for >12 hours to allow for mixing of the gases. In order to generate the precursor bromoform gas, liquid bromoform (Aldrich, 99+%) was added to a bubbler and the known vapor pressure of bromoform ($\sim$5 Torr ($\sim$0.7 kPa) at 298 K) was entrained in $\sim$2 atm ($\sim$203 kPa) of bath gas (Simnikov 1941; Linstrom & Mallard 2001).

Individual gases were combined in a mixing manifold with Mass Flow Controllers (MFC) (MKS, type 1179A) such that the final range of experimental gas compositions to be sent to the Laval nozzle apparatus was $\sim$0.1 - 1.0% CH_2O, $\sim$0.01% $CHBr_3$, and $\sim$99% Ar or N_2 bath gas. The absolute concentration of formaldehyde in each final mixture was also determined via UV absorption measurements, since formaldehyde gas slowly reformed solid polymers which sufficiently coated the walls of the MFC to render the calibration of the flow rate unusable within a day of measurements. The gas mixtures were sampled from the tubing between the mixing manifold and the pulsed valves and measured in a custom-built 1 m path length UV absorption cell. The absorption light source was a UVB lamp (EXOTERRA, UVB200) with continuous output between $\sim$290 - 350 nm. Absorption spectra collected from the UV/Vis spectrometer (Ocean Optics, HR4000CG-UV-NIR) with 0.75 nm resolution were integrated for 2 seconds and 4 spectra traces were averaged in order to generate an averaged spectrum that was utilized to determine the concentration of formaldehyde

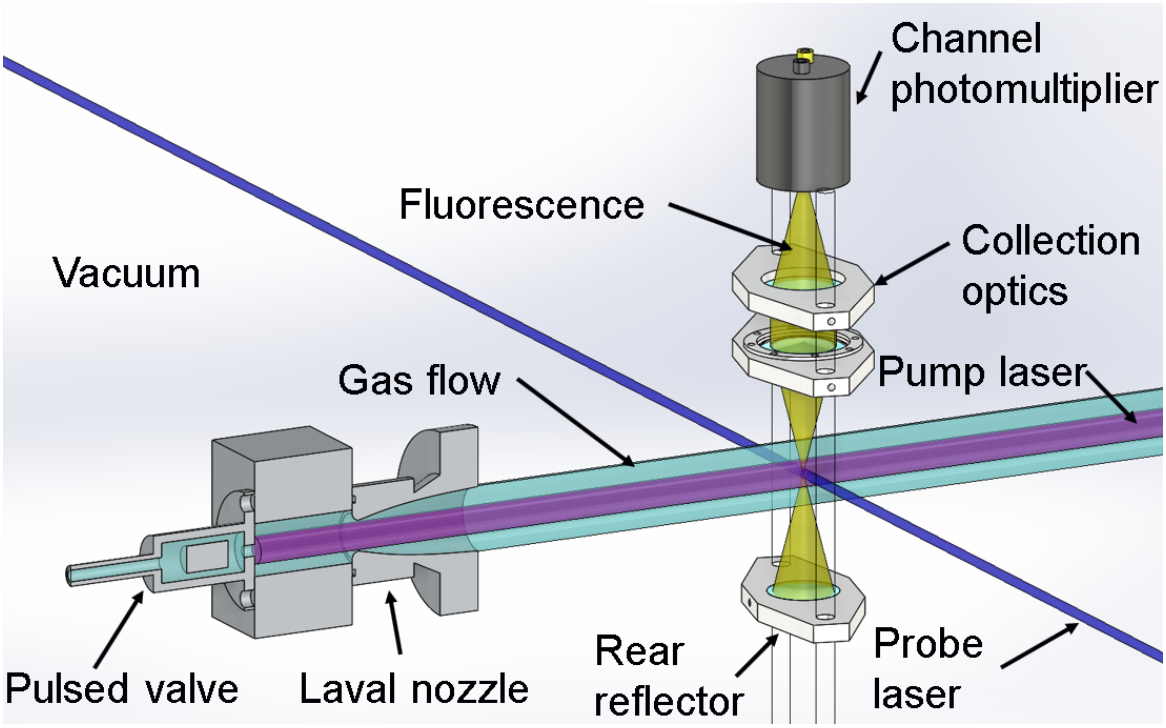


Figure 1. Schematic of the pulsed Laval nozzle apparatus and the PLP-LIF technique. Reprinted and adapted with permission from Heard, D. E. 2018, AcChR, 51, 2620. Copyright 2018 American Chemical Society.

for each gas mixture. The pressure of each gas mixture in the absorption cell was measured by a capacitance manometer (MKS, 0 - 100 PSIA (0 - 689 kPa)) to be ∼1.2 atm (∼122 kPa), approximately equal to the pressure behind the pulsed valves from where the gas mixtures were sampled. Representative UV absorption measurements of CH_2O are shown in the appendix. It was found that the half-life of formaldehyde in a cylinder of initially ∼4.4% formaldehyde in nitrogen was about 4 days.

After the gas ballast, each final mixture of gas was pulsed at 5 Hz through 2 solenoid valves (Parker, series 9) into the 1 cm^3 pre-expansion reservoir of the Laval nozzle apparatus. The use and characterization of this apparatus was described in detail previously (Taylor et al. 2008; Shannon et al. 2010; Caravan et al. 2014; Gómez Martín et al. 2014; Shannon et al. 2014) so only a brief description is given here. Each pulse of gas underwent a controlled expansion through a custom-made, axisymmetric, Laval nozzle into a vacuum chamber at 0.3 - 2 Torr (40 - 267 Pa) resulting in a thermalized cold gas flow. A range of nozzles with Mach numbers between 5.00 and 2.49 were employed during the experiments to achieve flow temperatures between 30 - 134 K. The density and temperature of the flows were verified with impact pressure measurements as well as by fits of CH LIF rotational temperature measurements to spectra generated in the simulation software package LIFBASE (Luque & Crosley 1999). Each pulse of gas was evacuated from the vacuum chamber by two Roots blower vacuum pump systems in parallel: a Roots blower (Leybold RUVAC 251) backed by a rotary pump (Leybold D65B) and a Roots blower (Edwards EH250) backed by a rotary pump (Edwards ED660). The pressure in the vacuum chamber was monitored by a capacitance manometer (Leybold, type CTR90, 0 - 10 Torr (0 - 1.3 kPa)).

Kinetics experiments in the cold gas flow were carried out with the PLP-LIF technique. In order to initiate the reaction of CH with CH_2O, the $CHBr_3$ precursor was photolyzed co-linearly with the nozzle axis with the output of an excimer laser (Lambda Physik, LPX200) at 248 nm, the "Pump laser" in Figure 1, generating a uniform density of CH radicals.

$$CHBr_3 + 3\,h\nu_{248nm} \longrightarrow CH + Br + Br_2, \tag{10a}$$

$$CHBr_3 + 3\,h\nu_{248nm} \longrightarrow CH^* + Br + Br_2, \tag{10b}$$

$$CH^* \xrightarrow{k_{rel}^{emission}} CH + h\nu, \tag{11}$$

$$CH^* + Q \xrightarrow{k_{rel}^{quench}} CH + Q^*, \tag{12}$$

$$k'_{rel} = k_{rel}^{emission} + k_{rel}^{quench}[Q], \tag{13}$$

where CH^* is rotationally, vibrationally, and/or electronically excited CH and k'_{rel} is a simplified first-order rate coefficient approximating many pathways of electronic, vibrational, and rotational relaxation of CH^* to CH, and Q is any species which collisionally relaxes CH^* (Lindner et al. 1998; Zou et al. 2004). The transient relative concentration of CH radicals was then monitored via the $Q_2(1)$ rotational line of the $B^2\Sigma - X^2\Pi$ (1,0) vibronic transition at 363.569 nm by probing with a pulsed Nd:YAG (Litron, LYP 664-10) pumped dye laser (Sirah, Cobra Stretch), the "Probe laser" in Figure 1. The probe laser beam was passed transversely through the gas flow, perpendicularly crossing the pump laser at the furthest distance from the exit of the nozzle before the flow broke up due to turbulence (typically ∼10 - 25 cm depending on the nozzle). The resulting fluorescence was focused with a series of lenses through two optical filters: a bandpass Filter at 400 nm with a Full Width at Half Max (FWHM) of 40 nm (Thorlabs, FB400-40) and a clear acrylic ∼400 nm long-pass filter (Perspex) removing CH(B-X)(0,0) emission at ∼ 390 nm and selecting the CH(B-X)(1,1) at ∼ 404 nm in order to minimize CH^* emission from $CHBr_3$ photolysis at pump-probe time delays at $\lesssim 1\mu s$. The filtered fluorescence was then collected by a temporally gated Channel PhotoMultiplier (CPM) (PerkinElmer, C1952P) with spectral response over 165-750 nm. The signal from the CPM was then digitized and integrated on an oscilloscope (LeCroy, Waverunner LT264) and the integrated signal was sent to a custom LabVIEW program. This LabVIEW program also controlled a digital delay generator (BNC, Model 555) which controlled the timing of the experiment.

3. EXPERIMENTAL RESULTS AND DISCUSSION

In order to determine the temperature-dependent rate coefficients for the loss of CH due to reaction with CH_2O, the pseudo-first-order rate coefficients, k_{obs}, were first measured at multiple concentrations of CH_2O for a given temperature. The relative temporal evolution of CH was monitored by integrating CH LIF while randomly varying the pump-probe time delay for each gas pulse up to the longest time delay in which nascent CH, generated in the flow at the exit of the nozzle, took to reach the probed region of the flow (∼100 - 300 μs depending on the nozzle). This process was repeated so that the CH signal at each time delay was averaged from at least 4 laser shots. Representative traces of integrated CH LIF versus time for several CH_2O concentrations are shown in Figure 2.

In each CH trace, following the instantaneous production via Reaction 10a, there was a fast rise ($\lesssim$5 μs) due to relaxation of excited CH^*, formed by Reaction 10b, into the rovibrational level of the $X^2\Pi$ ground state probed via LIF, followed by an exponential decay due to both the diffusion of CH out of the probe laser beam volume:

$$CH \xrightarrow{k_{diff}} (\text{diffusive loss}), \tag{14}$$

and reaction of CH primarily with CH_2O, Reaction 1, and also CH with other species:

$$CH + X_i \xrightarrow{k_i^{other}} \text{products}, \tag{15}$$

where X_i is each non-reagent species i: namely N_2 (when N_2 was present as the bath gas), and also the precursor $CHBr_3$, one and two-photon photolysis products of $CHBr_3$, and as stated by the manufacturer, the $CHBr_3$ stabilizer 2-methyl-2-butene, which was present at 60-120 ppm in the $CHBr_3$ liquid. The observed pseudo-first-order rate coefficient for the loss of CH, k_{obs}, is then:

$$\begin{aligned} k_{obs} &= k_1[CH_2O] + k_{diff} + \sum_{i=1}^{N} \left([X_i]k_i^{other}\right) \\ &= k_1[CH_2O] + k_{int}, \end{aligned} \tag{16}$$

where N is the total number of non-reagent species in the cold gas flow. For each CH trace, the average background integrated LIF signal was determined by averaging the integrated LIF signal at negative pump-probe time delays. Each CH trace was then corrected by subtracting the average background signal, and then fitted utilizing a biexponential

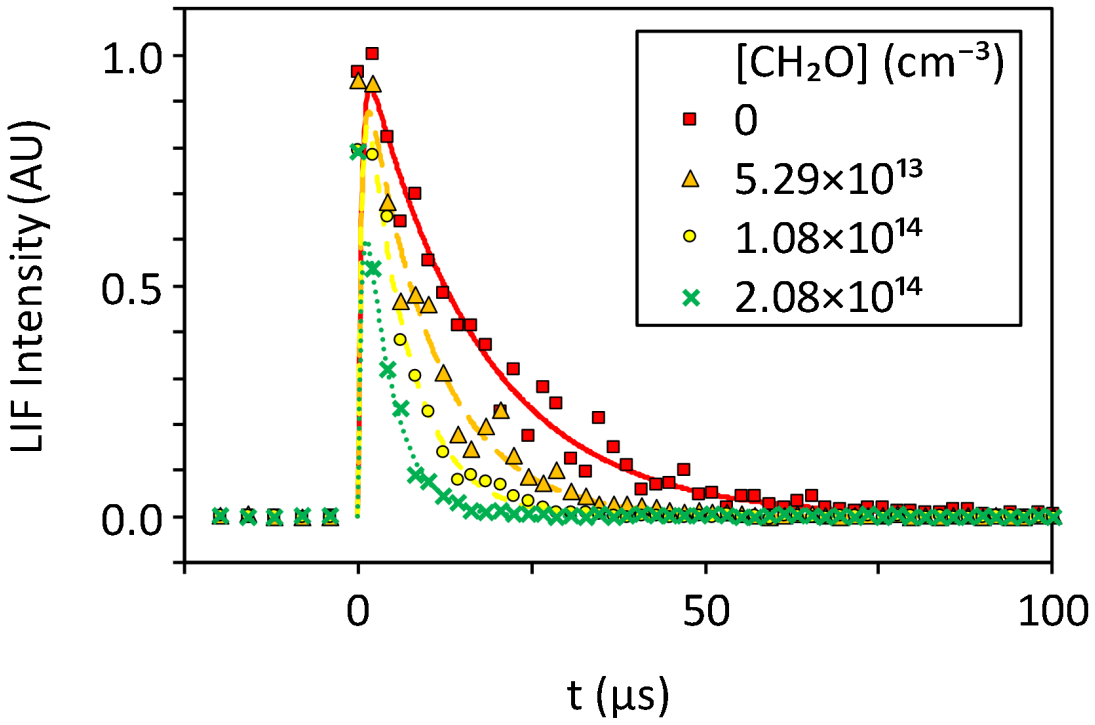


Figure 2. Representative transient CH integrated LIF traces utilized to determine the pseudo-first-order rate coefficients for loss of CH at 133 K and $[N_2] = 1.07 \times 10^{17}$ cm^{-3}, together with biexponential fits to the data for various concentrations of CH_2O.

function, given by Equation 18, where the observed pseudo-first-order rate coefficients of the exponential rise (k'_{rel}) and exponential decay (k_{obs}) were the fitted parameters and allowed to vary from trace to trace:

$$I(t) = f_1 e^{-k_{obs}t} - f_2 e^{-k'_{rel}t} \propto [CH]_t, \tag{17}$$

where

$$[CH]_t = \left[[CH]_{t=0} + \frac{k'_{rel}}{k'_{rel} - k_{obs}}[CH^*]_{t=0}\right] e^{-k_{obs}t} - \left[\frac{k'_{rel}}{k'_{rel} - k_{obs}}[CH^*]_{t=0}\right] e^{-k'_{rel}t}, \tag{18}$$

$I(t)$ is the time dependent LIF signal, $[CH]_{t=0}$ and $[CH^*]_{t=0}$ are the initial concentrations of CH and CH*, and f_1 and f_2 are fitted constants since the initial concentrations of $[CH]_{t=0}$ and $[CH^*]_{t=0}$ as well as the values of k'_{rel} are not all known under the experimental conditions in this work. The values of k_{obs} obtained from biexponential fits were also compared to values obtained by fitting single exponential decay curves starting after ~20 μs in the experimental traces, and these k_{obs} values were equivalent to those of the biexponential fits to within statistical significance. Each averaged CH trace was re-collected at least 5 times, and the fits of k_{obs} for these traces were averaged to obtain a $\bar{k}_{obs}$ value for each $[CH_2O]$.

$$\bar{k}_{obs} = \frac{1}{N}\sum_{i=1}^{N} k_{obs,i}, \tag{19}$$

where N is the number of fit traces and $k_{obs,i}$ is each fit i. The average values of fits of the rate of loss of CH, $\bar{k}_{obs}$, minus the intercept, k_{int} in Equation 16, versus $[CH_2O]$ are shown in Figure 3. The fitted value of k_{int} for each second order plot was between 8,000 $\lesssim k_{int}$ (s^{-1}) $\lesssim$ 60,000, shown in Figure 9 of Appendix B. Since all values of k_{int} in Ar were $\lesssim 8,000$ s^{-1}, the reaction CH + N_2 was estimated to account for up to ~52,000 s^{-1} of k_{int}.

For a given temperature, $\bar{k}_{obs}$ values increased linearly with $[CH_2O]$ until the formation of formaldehyde dimers, $(CH_2O)_2$, and higher order oligomers, $(CH_2O)_{n>2}$, began to occur, which resulted in the curving over of the second

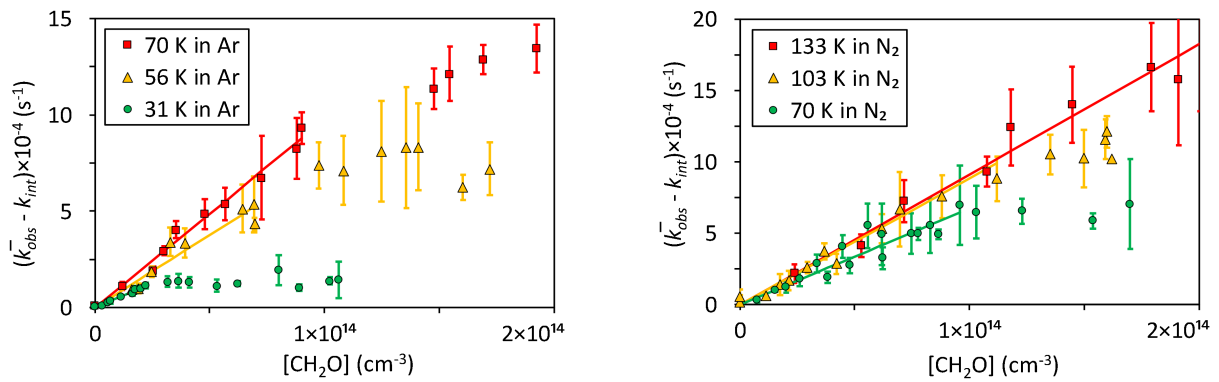


Figure 3. Intercept-subtracted average rate of loss of CH (Equations 16 and 19) versus the concentration of formaldehyde at various temperatures along with linear fits utilizing Equation 16 at each temperature. Error bars represent one standard deviation of fits of k_{obs} from at least 5 experimental CH temporal traces. The corresponding plots without subtraction of the k_{int} values are shown in Figure 9 of Appendix B.

order plots of $\bar{k}_{obs}$ vs [CH_2O] at the largest [CH_2O] values (i.e. the slowing or cessation of the increase in $\bar{k}_{obs}$ with [CH_2O]). The negative curvature of $\bar{k}_{obs}$ at higher [CH_2O] implies that formaldehyde dimers do not react fast enough with CH to counterbalance the loss of CH_2O monomers, and hence k_{obs}, due to dimerization. Therefore, the linear fits of $\bar{k}_{obs}$ versus [CH_2O] only included $\bar{k}_{obs}$ values from experiments where [CH_2O] was low enough such that no significant dimerization had occurred, where there was no significant curvature of $\bar{k}_{obs}$ versus [CH_2O]. The slopes of the linear fits represent the rate coefficient, $k_1(T)$, for Reaction 1 at a given temperature. Values of $k_1(T)$ with the corresponding experimental conditions are shown in Table 1. Measurements of $k_1(T)$ were repeated at 31 K and 70 K in order to verify experimental reproducibility. Values of $k_1(T)$ were found to have a positive temperature dependence over the range 31 < T < 133 K, and were also found to be independent of pressure at 70 K over a factor of 4.3 change in bath gas density (either N_2 or Ar) from $N_{total} = 2.58 \times 10^{16} - 11.18 \times 10^{16}$ cm^{-3}. Fit values of $k_1(T)$ versus T are shown in Figure 4 including measurements from Zabarnick et al. (1988) over the temperature range 300 - 670 K. Experiments from Zabarnick et al. (1988) measured the partial pressure of CH_2O manometrically before mixing gases in order to determine each [CH_2O], but did not use UV absorption to determine each [CH_2O].

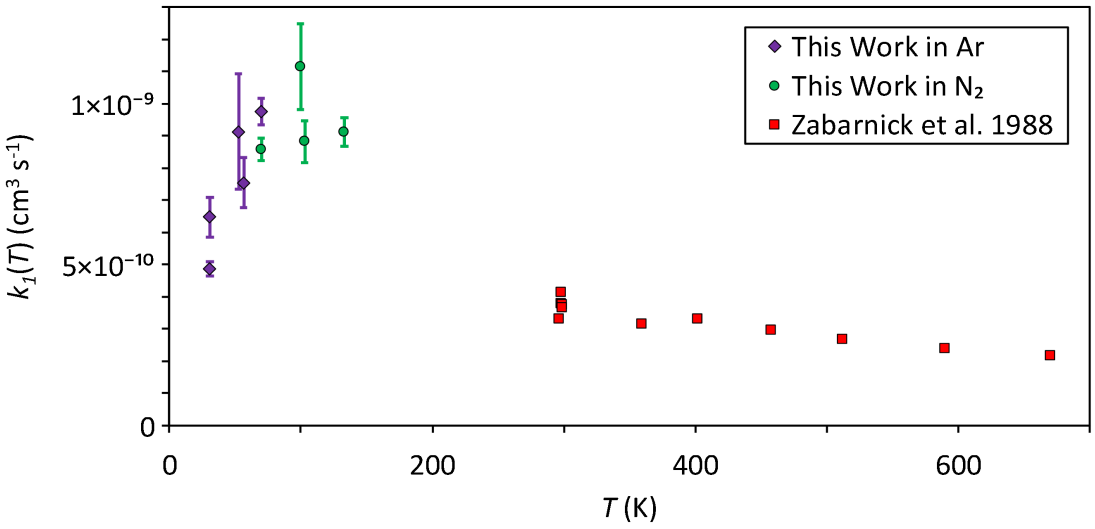


Figure 4. Measured values of $k_1(T)$ versus temperature. The error bars of each value of $k_1(T)$ from this work represent the error in the fitted slope of each second-order plot and do not include systematic errors.

Table 1. Rate coefficients and experimental conditions for CH + CH_2O.

T (K)	Bath Gas	N_{total} (10^{16} cm^{-3})	$k_1(T)$ (10^{-10} cm$^3 s^{-1}$)
31 ± 2	Ar	3.24 ± 0.24	4.86 ± 0.22
31 ± 2	Ar	3.24 ± 0.24	6.48 ± 0.62
53 ± 4	Ar	7.04 ± 0.74	9.13 ± 1.80
57 ± 8	Ar	8.14 ± 1.67	7.55 ± 0.79
70 ± 11	Ar	11.18 ± 2.54	9.75 ± 0.42
70 ± 2	N_2	2.58 ± 0.14	8.59 ± 0.35
100 ± 6	N_2	6.03 ± 0.84	11.15 ± 1.34
103 ± 10	N_2	6.80 ± 1.57	8.82 ± 0.66
133 ± 13	N_2	10.70 ± 3.50	9.13 ± 0.45

NOTE— The error of each $k_1(T)$ value represents the error in the fitted value of the slope of $\bar{k}_{obs}$ versus [CH_2O] and does not include systematic errors. The errors in each value of T and N_{total} were calculated by first taking pitot pressure measurements in the cold flow along the axis of the nozzle, converting these values to temperature and density using thermodynamic relations, and then taking the standard deviation of these values.

Zabarnick et al. (1988) observed a mild negative temperature dependence of $k_1(T)$ versus T between 298 - 670 K. Since a positive temperature dependence of $k_1(T)$ between 31 - ∼100 K was observed in our experiments, the change from the positive temperature dependence to the negative temperature dependence of $k_1(T)$ must occur between ∼100 - 298 K, suggesting that the reaction mechanism changes in this range. If $k_{coll}(T)$ is calculated using classical capture theory, Equation 5, with the constants given in Table 2, and plotted versus temperature, as in Figure 5, then the values of $k_{coll}(T)$ agree fairly well with the experimental values of $k_1(T)$ near 100 K, suggesting that the reaction has reached the collision limit.

According to the CCT model, shown as a solid black curve in Figure 5, values of $k_1(T)$ cannot be larger than the limiting values in which every collision between CH and CH_2O results in a reaction. Therefore, the negative temperature dependence of $k_1(T)$ observed between 300 - 670 K should not be extrapolated below ∼150 K where the collision limit is reached. Furthermore, since the linear addition of the strengths of $D-D$, $Disp$, and $D-iD$ forces is somewhat different than the calculation of a long range potential with high level *ab initio* methods, and since there is always some error in experiments, it is not surprising that there are measured $k_1(T)$ values that are slightly greater than the first order estimate of the collision limit, $k_{coll}(T)$. At temperatures below ∼100 K, calculated values of $k_{coll}(T)$ diverge from measured $k_1(T)$ values, likely due to the limitations of classical capture theory, Equation 5, in not adequately describing $D-D$ and $D-Q$ interactions at these temperatures. When studying similar, diatom-diatom systems with the more rigorous AC approach, Clary et al. (1993) observed a temperature dependence of $\sim T^{1/6}$ near 0 K and $\sim T^{-1/6}$ at higher temperatures with a maximum at a temperature ($1 \lesssim$ T (K) $\lesssim 40$) which varied for reactions with differing ground electronic states. While AC theory calculations have been shown to predict similar temperature dependencies as those measured for $k_1(T)$ in this work, AC theory has not been able to match experimental rate coefficient values to better than a factor of 2. Additionally, it is possible that some other mechanism is causing $k_1(T)$ to have values less than the collision limit below ∼100 K. However, the mechanisms governing the negative temperature dependence of $k_1(T)$ above ∼100 K would have led to a further increase in $k_1(T)$ at lower temperatures if not for the collision limit. A new mechanism would have to explain why $k_1(T)$ has a positive temperature dependence below ∼100 K when there are strong mechanisms that would cause a negative temperature dependence. It is instead more likely that $k_1(T)$ is still governed by the collision limit below ∼100 K, and that the collision limit has a positive temperature dependence.

Table 2. Parameters used to calculate $k_{coll}(T)$ between CH and CH_2O.

Molecule	Dipole Moment		Polarizability	Ionization Energy	
	μ_n		α_n	I_n	
	(Debye)	(C cm)	(cm^3)	(eV)	(J)
CH	1.46	4.87×10^{-28} [1]	2.40×10^{-24} [3]	10.640	1.70×10^{-18} [5]
CH_2O	2.33	7.77×10^{-28} [2]	2.77×10^{-24} [4]	10.8887	1.74×10^{-18} [6]

References— [1]Phelps & Dalby (1966); [2]Nelson Jr et al. (1967); [3]Manohar & Pal (2007); [4]Olney et al. (1997); [5]Herzberg & Johns (1969); [6]Niu et al. (1993)

If the fit of the measured negative temperature dependence of $k_1(T)$ between 300 - 670 K is extrapolated to 133 K, and then a temperature dependence of $T^{1/6}$ is applied below 133 K, the experimental data are reasonably represented as shown in Figure 6 by the dotted brown curve. Furthermore, the total range of measured values of $k_1(T)$ between 31 - 670 K could be fit to within 28% to the modified Arrhenius equation, Equation 3. Note that this fit should not be used for prediction of the rate coefficient outside of the range of temperatures of 31 - 670 K. If instead of following an extrapolation of the modified Arrhenius curve, the rate coefficients were to follow a $T^{1/6}$ temperature dependence below 30 K, as predicted by adiabatic capture theory, the value given by the modified Arrhenius equation, Equation 3, would be incorrect by a factor of ~140 at 10 K. Additionally, an $A \times T^n$ fit was performed of the data between 31 - 133 K which indicated that the measured positive temperature dependence ($n = 0.32 \pm 0.11$) in this temperature range may be more appropriate than a $T^{1/6}$ dependence. The $A \times T^n$ fits are consistent with the form of the temperature dependence of the collision rate coefficients at the limit of $T \to 0$ calculated with rotationally adiabatic capture theory (Stoecklin et al. 1991; Clary et al. 1993). However, the maximum value in the rate coefficients measured in this work occurred near $T_{max} = 100$ K (for CH $^2\Pi$ + CH_2O $^1A_1$) while the maximum calculated for another somewhat electronically similar doublet+singlet system (OH $^2\Pi$ + HBr $^1\Sigma$) occurred at $T_{max} = 20$ K. This difference in T_{max}

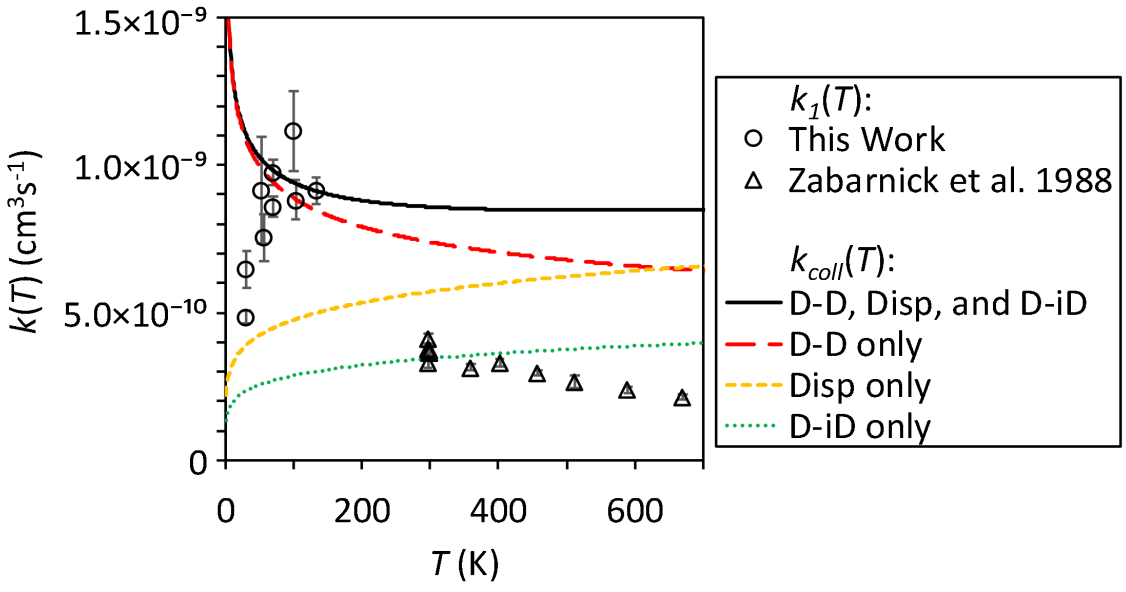


Figure 5. Measured values of $k_1(T)$ versus temperature compared with the calculated $k_{coll}(T)$ curve, Equation 5, and various relative contributions toward $k_{coll}(T)$. For "$D-D$ only," "$Disp$ only," and "$D-iD$ only" curves, $k_{coll}(T)$ was calculated with $C_6 = C_6^{D-D}$, $C_6 = C_6^{Disp}$, and $C_6 = C_6^{D-iD}$ respectively, Equations 7-9, in order to show the relative contribution of each intermolecular force to the total $k_{coll}(T)$. The error bars of each $k_1(T)$ value from this work represent the error in the fit value of the slope of each second-order plot and do not include systematic errors.

Table 3. Modified Arrhenius equation, Equation 3a, parameters from fits to experimental values of $k_1(T)$

Temperature Range (K)	Curve in Figure 6	A $(cm^3 s^{-1})$	τ (K)	n (Unitless)	E_a/k_B (K)
31 - 670	Brown dotted curve [1]	$(7.68 \pm 4.95) \times 10^{-7}$	1[a]	-1.26 ± 0.11	91.83 ± 10.66
298 - 670	Black curve [2]	$(1.57 \pm 0.14) \times 10^{-10}$	1[a]	0[a]	-260 ± 30
300 - 3000	Blue long dashed curve [3]	7.62×10^{-10}	1[a]	-0.32	-386
31 - 133	Orange dot-dot-dash curve [1]	$(4.20 \pm 0.23) \times 10^{-10}$	1[a]	$1/6$[a]	0[a]
31 - 133	Yellow short dashed curve [1]	$(2.15 \pm 1.03) \times 10^{-10}$	1[a]	0.32 ± 0.11	0[a]

References— [1]This work; [2]Nguyen et al. (2014); [3]Zabarnick et al. (1988);

[a] Value held constant during fit.

is likely due to differences in the electronic effects in the long-range potential between CH + CH_2O (Clary et al. 1993). Additionally, the maximum value of $k_1(T)$ is somewhat uncertain due to the uncertainty of the experimental measurements and lack of experimental measurements between 133 - 298 K. Values for parameters of the best fit functions shown in Figure 6 are given in Table 3. Furthermore, values for parameters from Table 3 were converted from fits where $\tau = 1$ to $\tau = 300$ using Equation 4 and are given in Table 4.

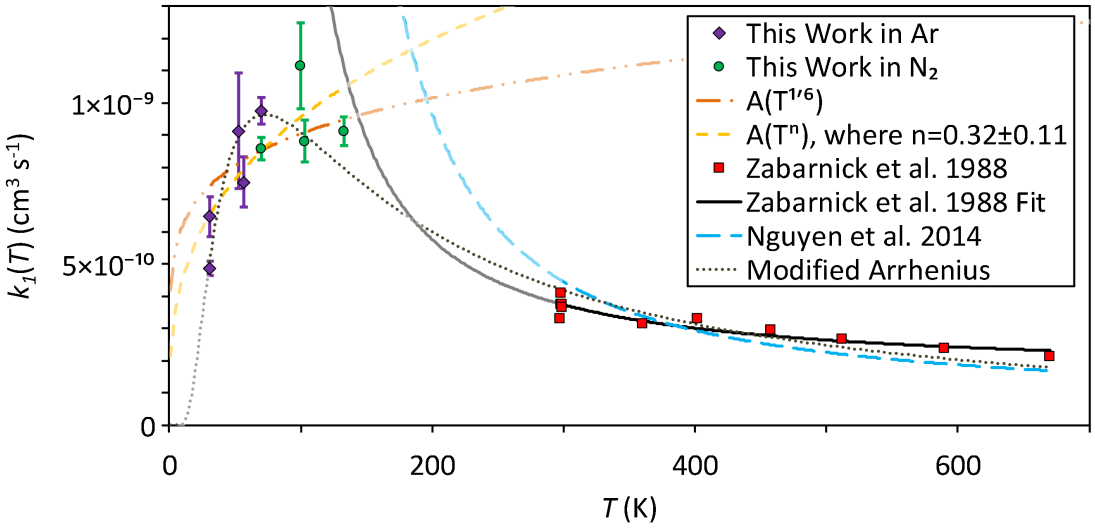


Figure 6. Measured values of $k_1(T)$ versus temperature together with fits using several approaches. Extrapolations of fit curves beyond measured values of $k_1(T)$ are shown with a lightened color of each respective fit curve. The error bars of each $k_1(T)$ value from this work represent the error in the fit value of the slope of each second-order plot and do not include systematic errors. The red square data points and the black fit curve were taken from Zabarnick et al. (1988) and the blue long dashed curve was taken from Nguyen et al. (2014).

Table 4. Parameters from Table 3 converted to modified Arrhenius, Equation 3a, fits where $\tau = 300$ using Equation 4.

Temperature Range (K)	Curve in Figure 6	A $(cm^3 s^{-1})$	τ (K)	n (Unitless)	E_a/k_B (K)
31 - 670	Brown dotted curve [1]	5.81×10^{-10}	300[a]	-1.26	91.83
298 - 670	Black curve [2]	1.57×10^{-10}	300[a]	0[a]	-260
300 - 3000	Blue long dashed curve [3]	1.23×10^{-10}	300[a]	−0.32	−386
31 - 133	Orange dot-dot-dash curve [1]	1.09×10^{-9}	300[a]	1/6[a]	0[a]
31 - 133	Yellow short dashed curve [1]	1.33×10^{-9}	300[a]	0.32	0[a]

References— [1]This work; [2]Nguyen et al. (2014); [3]Zabarnick et al. (1988);

[a] Value held constant during fit.

4. IMPACT ON CALCULATED ABUNDANCES IN ASTROPHYSICAL ENVIRONMENTS

The newly measured and theoretically calculated rate coefficients were used to investigate the impact of the CH + CH_2O reaction on the abundances of CH_2O, H_2CCO, and HCO and compared these to the calculated abundances without the new coefficients, using the UMIST Rate12 database (McElroy et al. 2013). The detailed parameters used in our calculations are given in Table 5, where 'Rate12' refers to the UMIST Database which includes only the HCO + CH_2 channel (Reaction 1c), 'CT' to the $T^{1/6}$-dependent rate coefficient based on capture theory, and 'MA' to the modified Arrhenius fit to the experimental data over the 31–670 K range (see Figure 6).

4.1. *Dark Interstellar Clouds*

We have investigated the implications of our newly measured rate coefficients in a model of a dark interstellar cloud with a visual extinction of 10 mags. We have modeled the gas-phase chemistry of two separate densities, $n(H_2) = 10^4$ and 10^5 cm^{-3}, each at temperatures of 10, 20 and 30 K, and for each of the three parameterizations of the rate coefficient given in Table 5. We used the low-metal elemental abundances believed to be appropriate for dark clouds (McElroy et al. 2013).

We have looked, in particular, at the abundances of CH and CH_2O as well as the main astronomically observable products of the reaction, CO, HCO, CH_3 and H_2CCO. Our calculations show that the abundances of the reactants CH and CH_2O are unchanged in the models as Reaction 1 represents only a minor loss of these species at all times, densities and temperatures. This is not surprising as CH is destroyed rapidly in reaction with species more abundant than formaldehyde, in particular the atoms O, N and H. Formaldehyde is predominantly destroyed by fast proton transfer reactions followed by dissociative recombination with electrons.

Similarly, the products of the title reaction have abundances which do not significantly differ from those in the Rate12 model, with the exception of H_2CCO which shows a small increase in abundance at early times, that is less than 2×10^5 yr, at all temperatures for $n(H_2) = 10^5$ cm^{-3} shown in Figure 7. In the UMIST database, the products

Table 5. Parameters for Equation 3b used in calculating temperature-dependent rate coefficients for the CH + CH_2O reaction.

Reaction	Products	Rate12			CT			MA		
		α	β	γ	α	β	γ	α	β	γ
1c	HCO + CH_2	9.21×10^{-12}	0.70	2000	2.18×10^{-11}	0.17	0.0	1.11×10^{-11}	-1.26	91.83
1a	H_2CCO + H	-	-	-	8.94×10^{-10}	0.17	0.0	4.76×10^{-10}	-1.26	91.83
1b	CH_3 + CO	-	-	-	1.74×10^{-10}	0.17	0.0	9.30×10^{-11}	-1.26	91.83

Note— Parameters for models based on capture theory (CT) and modified Arrhenius (MA) fits were calculated using fit curve parameters given in Table 4 where the alpha value for each channel was scaled according to the theoretical 300 K yields of Reactions 1a-1c.

of the title reaction are assumed to be CH_2 and HCO with an activation energy barrier of 2000 K (Mitchell 1984), taken from the compilation by Westley (1980).

Nguyen et al. (2014) determined that the major molecular product in the title reaction was ketene which thus provides a new route when compared to the UMIST Rate12 database. The impact of this new route is seen only in the higher density models at early times (Figure 7) where we find that between 8 and 21% of ketene is formed by this reaction. The largest contributions, 16–21%, to ketene formation occur at T = 30 K. In all cases, the percentage contribution is larger for the CT rate coefficient than for the MA fit to the laboratory data. Additionally, at 10 K the MA model yields unnoticeable differences to the H_2CCO abundance while the CT model yields a similar contribution to the H_2CCO abundance as in the 30 K model. This is due to the divergence of the MA and CT fit curves below 30 K. The increases in the ketene fractional abundance are relatively modest, however, with its maximum abundance, which occurs at 4–5 $\times$ 10^4 yr, varying as 4×10^{-8}, 5×10^{-8}, and 6×10^{-8} in the Rate12, MA, and CT models, respectively at 30 K and a change of a factor of $\sim$2 is observed in ketene at 10 K between CT and Rate12 models. If we use the smaller rate coefficient, 5 $\times$ 10^{-11} cm^3 s^{-1}, recommended by Baulch et al. (2005) for the O + C_2H_3 reaction in the range 250–2000 K (Section 1), then the maximum ketene fractional abundance is reduced slightly to 3–5 $\times$ 10^{-8}.

Finally, noting that Nguyen et al. (2014) suggested that the ketene yield in reaction 1a should increase with decreasing temperature, we ran a series of calculations with a 100%, rather than 82% yield for this channel. As expected, the increase in the H_2CCO abundance was minimal, limited to around 5–6% for the models presented here.

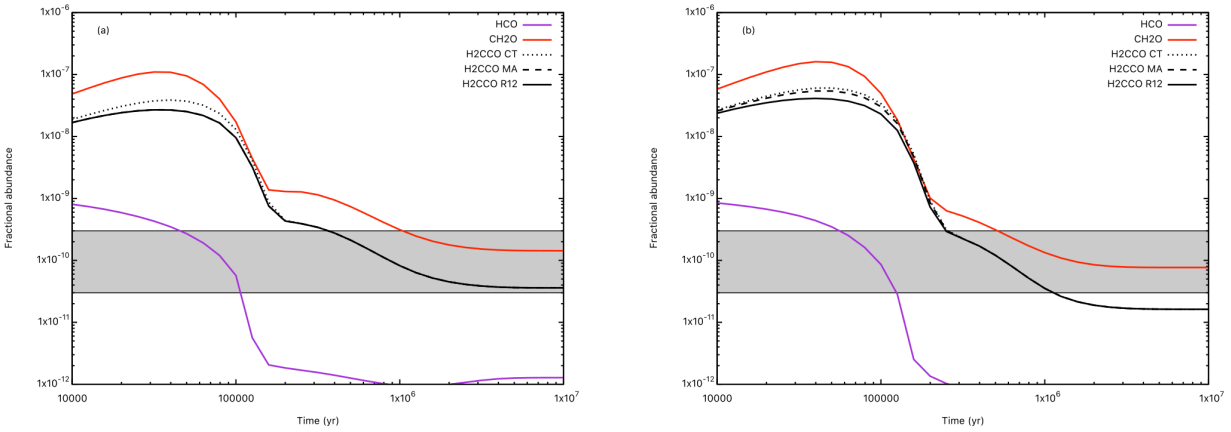


Figure 7. Abundances versus time of key reagents and products of the title reaction in cloud models with $n(H_2) = 10^5$ cm^{-3} and A_V = 10 mags for (a) T = 10 K and (b) T = 30 K. The abundances of HCO and CH_2O are identical in the CT, MA and R12 calculations. The grey box indicates the range in ketene abundances measured in dark clouds by Ruiterkamp et al. (2007) and Agúndez et al. (2010).

4.2. *Circumstellar Envelopes*

We have also investigated the implications of the parameterized rate coefficients listed in Table 5 on the chemistry within the CSEs of AGB stars. Our model is based on the publically available UMIST Database for Astrochemistry CSE model (McElroy et al. 2013)[1], where we changed the assumed gas temperature structure to a power-law,

$$T(r) = T_* \left(\frac{R_*}{r} \right)^{\epsilon}, \tag{20}$$

with T_* and R_* the stellar temperature and radius, and ϵ the exponent characterising the power-law (Van de Sande et al. 2018). We calculated a grid of models, where we varied over the mass-loss rate of outflow, $\dot{M} = 10^{-5}$ and 10^{-7} $M_\odot$ yr^{-1}, the stellar temperature T_* = 2000 and 2300 K, the power-law exponent ϵ = 0.5 and 0.7. We assume that stellar radius $R_* = 5 \times 10^{13}$ cm and a constant expansion velocity of 15 km s^{-1}. Both an O-rich and a C-rich outflow are investigated. The parent species and their initial abundances are taken from Agúndez et al. (2010).

[1] http://udfa.ajmarkwick.net/index.php?mode=downloads

The results are similar to those from the dark cloud models. We find that the inclusion of the CT and MA rate coefficients does not noticeably affect the abundance profiles of CH and CH_2O or any of the observable reaction products. The largest changes are seen for C-rich outflows because of the higher density of the reactants. For both C-rich and O-rich outflows, higher density outflows with a colder temperature structure, i.e. $T_* = 2000$ K and $\epsilon = 0.5$, result in larger changes. The column densities of the species considered change by maximally 2% relative to the Rate12 reaction rate coefficients in both the O-rich and C-rich CSE. These changes are too small to be observable. The largest change of ∼2% corresponds to the decrease in column density of CH_2O. The column density of H_2CCO increases by maximally 1%. The additional route to form ketene hence also increases its abundance in CSEs, albeit only very slightly due to the difference in physical structure of the outflow. Using a 100% yield for reaction channel 1a instead of 82% does not result in a larger increase of the ketene abundance. The column densities of the other products increase by less than 1%.

5. CONCLUSIONS AND PROSPECTS

Over the temperature range 31 - 133 K, rate coefficients for the reaction of CH + CH_2O, $k_1(T)$, have been determined to be very large such that the reaction is at the collision limit. Values of $k_1(T)$ near ∼100 K are among the largest measured rate coefficient values for a neutral-neutral gas phase reaction below 300 K (within the largest 4 of the 620 listed in the UMIST RATE12 database). $k_1(T)$ at 30 K is among the 10 largest rate coefficient values for a neutral-neutral gas phase reaction included in the UMIST RATE12 database (many of which are extrapolations from measurements of C atom reactions at 300 K). Below ∼70 K, measured values of $k_1(T)$ were observed to decrease with a decrease in temperature. This positive temperature dependence is not predicted by classical capture rate theory but is predicted by the more detailed adiabatic capture rate theory. The values of $k_1(T)$ have been parameterized both using a simple modified Arrhenius equation as well as using an $A \times T^{1/6}$ fit based on low temperature AC theory. These parameterizations were then added to the UMIST Rate12 astrochemical chemical network for two model scenarios: dark interstellar clouds and circumstellar envelopes. The change in CH_2O abundance in these two environments was essentially unchanged with our inputted $k_1(T)$, since formaldehyde is destroyed rapidly in reactions with ions and with other more abundant atoms and radicals than CH. However, the dominant molecular product from CH + CH_2O is ketene, H_2CCO, and significant abundance changes in ketene were observed in some of the model runs. The observation of a large rate coefficient decreasing with a decrease in temperature at temperatures relevant for interstellar space, as was measured for the reaction CH + CH_2O, might be more general than is presently acknowledged. Our extrapolation of $k_1(T)$ to T below our measured values has a large uncertainty, but this uncertainty would be significantly reduced if there was better theoretical understanding of collision rate theory at low T. Although AC theory and μj-VTST have been shown to calculate qualitatively correct temperature dependencies to within a factor of two for measured reaction rate coefficients of some systems at the collision limit, even better theoretical understanding of collision rate theory at low T would allow for higher confidence in extrapolation of fits of measured rate coefficients to lower temperatures. Until more experimental or theoretical results are available to extend the temperature range over which the rate coefficient is determined, we recommend that the MA fit (brown dotted curve in Figure 6) is applied over the range of $38.5 \leq T$ (K) ≤ 670 and the AT^n fit (yellow short dashed curve in Figure 6) is applied over the range of $0 \leq T$ (K) ≤ 38.5, if an extrapolation is to be made below 31 K, for example for use in astrochemical simulations. We recommend that these two parameterized fits be input, over their respective temperature ranges, into reaction databases such as UMIST Rate12 and the KIDA.

6. ACKNOWLEDGEMENTS

This project has received funding from the European Research Council (ERC) under the European Unions Horizon 2020 research and innovation programme (grant agreement No 646758). We would like to thank the mechanical and electronics workshops in the School of Chemistry at the University of Leeds for support. We would like to thank John Plane for helpful discussions on classical capture theory. TJM is grateful to the STFC for support through grant ST/P000321/1 and to the Institute for Theory and Computation for hospitality. MVdS acknowledges support from the Research Foundation Flanders (FWO) through grant 12X6419N. We would also like to thank two anonymous referees for their prompt response and insightful comments.

Software: LIFBASE (Luque & Crosley 1999)

Software: UDfA (McElroy et al. 2013)

APPENDIX

A. UV ABSORPTION

UV absorption spectra of formaldehyde gas were utilized in order to determine the concentration of formaldehyde in each final mixture of gas in low temperature kinetics measurements. Two representative UV absorption spectra are shown in Figure 8. In order to fit UV absorption spectra collected in this study, a least-squares minimization analysis was performed comparing the collected spectra to a modified version of a literature UV absorption spectrum. First, a high-resolution UV absorption spectrum from Smith et al. (2006a) was convoluted with a 0.75 nm Gaussian function in order to match the resolution of the spectrometer in this study. The convoluted spectrum was then linearly interpolated onto the wavelength grid of the spectra collected in this study. An initial guess of the number density of formaldehyde in the absorption cell, $N_{CH_2O}^{AbsCell}$ (cm^{-3}), was then utilized to convert absorbance, A, to absorption cross section, σ. A least-squares minimization analysis was then performed by varying the estimated $N_{CH_2O}^{AbsCell}$ in the data spectra in order to obtain a best fit of $N_{CH_2O}^{AbsCell}$, while the total pressure measured in the absorption cell was then utilized to calculate the total number density, $N_{total}^{AbsCell}$ (cm^{-3}). $N_{CH_2O}^{AbsCell}$ was then divided by $N_{total}^{AbsCell}$ in order to calculate the fraction of formaldehyde gas in the cell, and the value then adopted as the fraction of formaldehyde in the low temperature flows generated by the Laval nozzles. The statistical error in the fitted $N_{CH_2O}^{AbsCell}$ values were determined to be $\lesssim$2% by taking the standard error of the slope of $A/l^{AbsCell}$ versus σ^{lit} where $l^{AbsCell}$ is the path length, and A and σ^{lit} are the wavelength dependent absorbance values and literature cross section values from Smith et al. (2006a) respectively. However, for [CH_2O] values used in second order plots, Figure 3, the uncertainty was dominated by the ~10% uncertainty of the density of the cold flows.

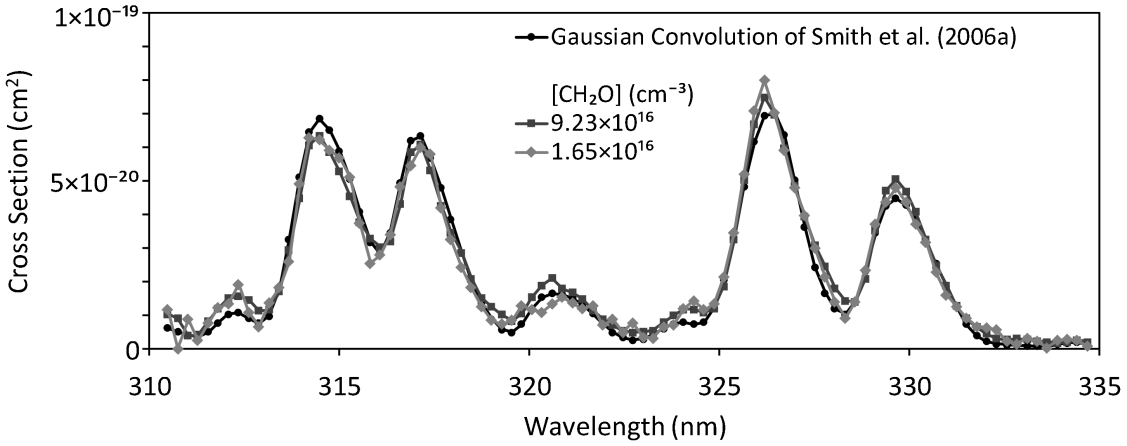


Figure 8. Absorption spectra of formaldehyde at various concentrations of CH_2O fitted to the convolution of a Gaussian function of 0.75 nm FWHM with a 0.0035 nm high resolution spectrum from Smith et al. (2006a).

B. SECOND ORDER PLOTS

Un-subtracted plots of the average value of fits of the rate of loss of CH ($\bar{k}_{obs}$) versus [CH_2O] are shown in Figure 9. The fitted k_{int} values from linear fits represent loss of CH due to diffusion as well as reaction with species besides CH_2O (primarily N_2 when present and, with probable minor contributions from the precursor $CHBr_3$, one and two-photon photolysis products of $CHBr_3$, and as stated by the manufacturer, the $CHBr_3$ stabilizer 2-methyl-2-butene, which was present at 60-120 ppm in the $CHBr_3$ liquid). Therefore, once differences in the rates of CH diffusion (due to differences in flow temperature and density) are subtracted from each k_{int}, the remaining contribution to k_{int} is primarily accounted for by the reaction of CH with N_2 (when N_2 was present in the flow field) to within the uncertainty of our k_{int} values when compared with low temperature rate coefficients for the reaction of CH + N_2 measured by Le Picard et al. (1998). The rate coefficients for three-body association of CH + N_2 from Le Picard et al. (1998) down to 53 K were of similar magnitude but somewhat smaller than those obtained through analysis of k_{int} values in this

work, however, there is a relatively high uncertainty in obtaining a rate coefficient for CH + N_2 from analysis of k_{int} values.

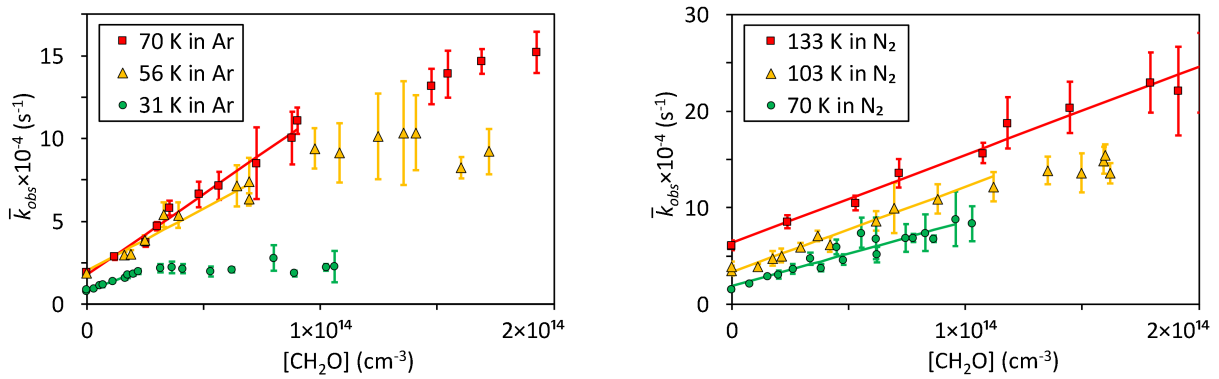


Figure 9. Average rate of loss of CH versus the concentration of formaldehyde at various temperatures along with linear fits at each temperature. Error bars represent one standard deviation of fits of k_{obs} from at least 5 experimental decay traces.

REFERENCES

Agúndez, M., Cernicharo, J., & Guélin, M. 2010, ApJL, 724, L133

Anderson, L. G., Lanning, J. A., Barrell, R., et al. 1996, Atmos. Env., 30, 2113

Atreya, S. K. 2010, Far. Dis., 147, 9

Baulch, D. L., Bowman, C. T., Cobos, C. J., et al. 2005, Journal of Physical and Chemical Reference Data, 34, 757

Canosa, A., Sims, I., Travers, D., Smith, I., & Rowe, B. 1997, A&A, 323, 644

Caravan, R. L., Shannon, R. J., Lewis, T., Blitz, M. A., & Heard, D. E. 2014, JCPA, 119, 7130

Carlier, P., Hannachi, H., & Mouvier, G. 1986, Atmos. Env. (1967), 20, 2079

Clary, D. 1994, AIP Conference Proceedings, 312, 405

Clary, D. C., Stoecklin, T. S., & Wickham, A. G. 1993, Far. Trans., 89, 2185

Cooke, I., & Sims, I. R. 2019, ACS Earth and Space Chemistry

Danks, A. C., Federman, S. R., & Lambert, D. L. 1984, A&A, 130, 62

Fenimore, C. 1971, Symposium (International) on Combustion, 13, 373

Georgievskii, Y., & Klippenstein, S. J. 2005, JChPh, 122, 194103

Gómez Martín, J., Caravan, R., Blitz, M., Heard, D., & Plane, J. 2014, JCPA, 118, 2693

Goulay, F., Trevitt, A. J., Meloni, G., et al. 2009, JAChS, 131, 993

Grosjean, E., Williams, E. L., & Grosjean, D. 1993, Air & Waste, 43, 469

Heard, D. E. 2018, AcChR, 51, 2620

Herzberg, G., & Johns, J. 1969, ApJ, 158, 399

Hirschfelder, J. O., Curtiss, C. F., & Bird, R. B. 1964, Molecular theory of gases and liquids (Wiley: New York)

Hudson, R. L., & Loeffler, M. J. 2013, ApJ, 773, 109

Krasnopolsky, V. A. 2009, Icarus, 201, 226

Le Picard, S. D., Canosa, A., Rowe, B. R., et al. 1998, Far. Trans., 94, 2889

Lindner, J., Ermisch, K., & Wilhelm, R. 1998, Chemical physics, 238, 329

Linstrom, P. J., & Mallard, W. 2001, NIST Chemistry webbook; NIST standard reference database No. 69, National Institute of Standards and Technology. https://webbook.nist.gov/

Luque, J., & Crosley, D. R. 1999, SRI international report MP, 99

Maity, S., Kaiser, R. I., & Jones, B. M. 2014, ApJ, 789, 36

Manohar, P. U., & Pal, S. 2007, CPL, 438, 321

Matthews, H. E., & Sears, T. J. 1986, ApJ, 300, 766

McElroy, D., Walsh, C., Markwick, A. J., et al. 2013, A&A, 550, A36

McKellar, A. 1941, Publ DAO, 7, 251

Miller, J. A., & Bowman, C. T. 1989, PrECS, 15, 287

Mitchell, G. F. 1984, ApJS, 54, 81

Muller, S., Combes, F., Guélin, M., et al. 2014, A&A, 566, A112

Nelson Jr, R. D., Lide Jr, D. R., & Maryott, A. A. 1967, Selected values of electric dipole moments for molecules in the gas phase, Tech. rep., National Standard Reference Data System-National Bureau of Standards

Nguyen, H. M. T., Nguyen, H. T., Nguyen, T.-N., Van Hoang, H., & Vereecken, L. 2014, JPCA, 118, 8861

Niu, B., Shirley, D. A., & Bai, Y. 1993, JChPh, 98, 4377

Nixon, C. A., Achterberg, R. K., Teanby, N. A., et al. 2010, Far. Dis., 147, 65

Oliveira, A. M., Lehman, J. H., McCoy, A. B., & Lineberger, W. C. 2016, JChPh, 145, 124317

Olney, T. N., Cann, N., Cooper, G., & Brion, C. 1997, Chem. Phys., 223, 59

Phelps, D., & Dalby, F. 1966, PhRvL, 16, 3

Phillips, L. F. 1992, PrECS, 18, 75

Potapov, A., Canosa, A., Jiménez, E., & Rowe, B. 2017, Angew.e Chem. Int. Ed., 56, 8618

Quack, M., & Troe, J. 1974, Ber. Bunsengesellschaft Phys. Chem., 78, 240

Ruiterkamp, R., Charnley, S. B., Butner, H. M., et al. 2007, Ap&SS, 310, 181

Rydbeck, O. E. H., Elldér, J., & Irvine, W. M. 1973, Nature, 246, 466

Sandell, G., Magnani, L., & Lada, E. A. 1988, ApJ, 329, 920

Saxena, P., Bhatnagar, S., & Singh, M. 2003, Bull. Astron. Soc. India, 31, 67

Shannon, R., Caravan, R., Blitz, M., & Heard, D. 2014, PCCP, 16, 3466

Shannon, R. J., Taylor, S., Goddard, A., Blitz, M. A., & Heard, D. E. 2010, PCCP, 12, 13511

Simnikov, I. 1941, Zh. Obshch. Khim., 14, 483

Sivakumaran, V., Hölscher, D., Dillon, T. J., & Crowley, J. N. 2003, PCCP, 5, 4821

Smith, C. A., Pope, F. D., Cronin, B., Parkes, C. B., & Orr-Ewing, A. J. 2006a, JCPA, 110, 11645

Smith, I. W. 1980, Kinetics and Dynamics of Elementary Gas Reactions: Butterworths Monographs in Chemistry and Chemical Engineering (Butterworth and Co)

Smith, I. W., Sage, A. M., Donahue, N. M., Herbst, E., & Quan, D. 2006b, Far. Dis., 133, 137

Snyder, L. E., Buhl, D., Zuckerman, B., & Palmer, P. 1969, PhRvL, 22, 679

Stoecklin, T., & Clary, D. 1995, Journal of Molecular Structure: THEOCHEM, 341, 53

Stoecklin, T., Dateo, C., & Clary, D. 1991, Far. Trans., 87, 1667

Taylor, S. E., Goddard, A., Blitz, M. A., Cleary, P. A., & Heard, D. E. 2008, PCCP, 10, 422

Troe, J. 1985, CPL, 122, 425

Tsang, W., & Hampson, R. F. 1986, JPCRD, 15, 1087

Turner, B. E. 1977, ApJ, 213, L75

Van de Sande, M., Sundqvist, J. O., Millar, T. J., et al. 2018, A&A, 616, A106

Viskari, E.-L., Vartiainen, M., & Pasanen, P. 2000, Atmos. Env., 34, 917

Wakelam, V., Loison, J. C., Herbst, E., et al. 2015, ApJS, 217, 20

Westley, F. 1980, Table of Recommended Rate Constants for Chemical Reactions Occuring in Combustion , Tech. rep., National Standard Reference Data System-National Bureau of Standards

Zabarnick, S., Fleming, J., & Lin, M. 1988, Symposium (International) on Combustion, 21, 713

Zou, P., Shu, J., Sears, T. J., Hall, G. E., & North, S. W. 2004, The Journal of Physical Chemistry A, 108, 1482